Available online at www.sciencedirect.com
ScienceDirect
Ceramics International 36 (2010) 483–490
CERAMICS INTERNATIONAL
www.elsevier.com/locate/ceramint

Preparation and characterization of neodymium-doped ceria electrolyte materials for solid oxide fuel cells

Yen-Pei Fu *, Sih-Hong Chen

Department of Materials Science and Engineering, National Dong-Hwa University, Shou-Feng, Hualien 974, Taiwan

Received 6 May 2009; received in revised form 3 August 2009; accepted 27 August 2009
Available online 23 September 2009

Abstract

The microstructure, thermal expansion, microhardness, indentation fracture toughness, and ionic conductivity of neodymium-doped ceria (NDC) prepared by coprecipitation were investigated. The results revealed that the average particle size (D_{BET}) ranged from 20.1 to 25.8 nm, crystallite dimension (D_{XRD}) varied from 17.5 to 20.7 nm, and the specific surface area distribution was from 31.25 to 40.27 m^2/g for neodymium-doped ceria stacking powders. Dependence of lattice parameter, a, versus dopant concentration, x, of Nd^{3+} ion shows that these solid solutions obey Vegard's rule as $a(x) = 5.4069 + 0.1642x$ for $Ce_{1-x}Nd_xO_{2-(1/2)x}$ for $x = 0.05$–0.25. For neodymium-doped ceria ceramics sintered at 1500 °C for 5 h, the bulk density was over 95% of the theoretical density. The maximum ionic conductivity, $\sigma_{800^\circ C} = 4.615 \times 10^{-2}$ S/cm, with the minimum activation energy, $E_a = 0.794$ eV was found for the $Ce_{0.75}Nd_{0.25}O_{1.875}$ ceramic. Trivalent, neodymium-doped ceria ceramics revealed high fracture toughness, the fracture toughness distribution was in the range of 6.236 ± 0.021 to 6.846 ± 0.017 MPa $m^{1/2}$. The high indentation fracture toughness of neodymium-doped ceria was attributed to crack deflection. Moreover, the porosity may influence the mechanical properties such as microhardness and fracture toughness. It was observed that as the porosity reduced, the microhardness and fracture toughness increased.

Keywords: A. Powders: chemical preparation; C. Fracture; C. Ionic conductivity; D. CeO_2; E. Fuel cells

1. Introduction

A solid oxide fuel cell (SOFC) is regarded as a highly efficient power-generation system for future applications. A typical high-temperature SOFC uses 8 mol% yttria-stabilized zirconia (YSZ) as the electrolyte and usually operated at temperatures in the range of 800–1000 °C to obtain the required high ionic conductivity. However, such high temperatures will lead to a reaction between the various components, thermal degradation or thermal expansion mismatch [1]. In order to reduce the operation temperature from 1000 to 800 °C or even lower, doped ceria has been considered as a possible solid electrolyte for intermediate temperature SOFCs [2]. The conductivity maximum in zirconia has been correlated with the minimum dopant level necessary to stabilize the high-temperature face-centered cubic (fcc) phase. Contrary to pure YSZ, $CeO_{2-\delta}$ has the fluorite structure and oxygen vacancies ($V^{\bullet\bullet}_O$) as the predominant ionic defect [3–5].

Pure CeO_2 ceramic is a poor oxide ion conductor. However, the ion conductivity of CeO_2 can be significantly improved by the substitution of the Ce^{4+} ion with some trivalent oxides, because the number of oxygen vacancies can be greatly increased as a result of charge compensation. The electrical conductivity in doped ceria is influenced through a complex relationship by several factors such as the dopant ion, the dopant concentration, the oxygen vacancy concentration, and the defect association enthalpy. Such a relationship is not simple point to point, but through a combination of several factors [6–8].

Materials used in SOFC system may be susceptible to fracture due to mechanical and thermal stresses resulting from fabrication and operation. Unfortunately, ceria-based materials possess poor mechanical strength, this may limit ceria-based ceramics for electrolyte applications [9,10]. The addition of a rare earth oxide to CeO_2 can slightly improve mechanical properties [10]. Chemical precipitation is a simple and feasible technique for synthesizing ultrafine ceramic powders with high sinterability [11,12].

* Corresponding author. Tel.: +886 3 863 4209; fax: +886 3 863 4200.
E-mail address: d887503@alumni.nthu.edu.tw (Y.-P. Fu).

0272-8842/$36.00
doi:10.1016/j.ceramint.2009.09.013

In the present study, we report the results of a systematic study of the lattice parameter, the microstructure, thermal expansion, microhardness, indentation fracture toughness and electrical properties of neodymium-doped ceria (NDC) produced by a coprecipitation process.

2. Experimental procedures

2.1. Sample synthesis

Solid solution $Ce_{1-x}Nd_xO_{2-(1/2)x}$ (x = 0.05, 0.10, 0.15, 0.20, 0.25) was synthesized by a previously reported coprecipitation method [11,12]. Stoichiometric amounts of cerium nitrate hexahydrate ($Ce(NO_3)_3{\cdot}6H_2O$), and neodymium nitrate hexahydrate ($Nd(NO_3)_3{\cdot}6H_2O$) were dissolved in distilled water. The final concentration of the stock solution was 0.2 M for Ce^{3+}. When the ammonia (NH_4OH) solution was added to the nitrate solution, precipitates started to form at pH = 9.5. The resulting precipitate mass was vacuum-filtered, washed three times with distilled water and finally ethanol. In order to produce soft-agglomerates of NDC powder, butanol solution was mixed with the precursor precipitate in a beaker and heated to 100 °C on a hot plate for 4 h. In this process, water in the precursor will be replaced with butanol, because the boiling point of butanol (118 °C) is higher than water (100 °C). This process will contribute to elimination of hard agglomerates during the powder drying stage. Finally, the precipitate mass was dried at 125 °C in an oven. The coprecipitated hydrate powder is decomposed to a polycrystalline oxide by heating to 600 °C for 2 h. The oxidation of Ce^{3+} to Ce^{4+} occurred during this stage. Dense components of the powder samples, of the individual compositions, were pellet formation and sintering at 1500 °C for 5 h with a programmed heating rate of 5 °C per minute and cooled at 3 °C per minute to room temperature. The densities of the sintered samples were all greater than 95% of theoretical value.

2.2. Characterization measurements

A computer-interface X-ray powder diffractometer (XRD; Model Rigaku D/Max-II, Tokyo, Japan) with Cu K_α radiation (λ = 0.15418 nm) was used to identify the crystalline phase and determine the crystallite size. Calculation of the lattice parameters was carried out using the four main reflections typical of a fluorite structure material with an fcc cell, corresponding to the (1 1 1), (2 0 0), (2 2 0), and (3 1 1) planes. The lattice parameter (a) of the doped cubic-ceria solid solution can be calculated using the follow relations:

$$d = \frac{\lambda}{2\sin\theta}; \qquad a = d\sqrt{h^2 + k^2 + l^2} \tag{1}$$

where d is the planar spacing, λ the wavelength of the radiation (λ = 0.15418 nm), θ the diffraction angle, and a is the lattice parameter.

The crystallite size (D_{XRD}) was calculated according to Scherer equation [13]. The measurements were calibrated using the half-width of a standard CeO_2 with a crystal size greater than 100 nm. The (1 1 1) plane reflection was used to calculate the crystallite size.

BET surface area measurements were made by nitrogen adsorption employing a Micromeritics ASAP 2010 instrument and calculated using the five point Brunauer–Emmett–Teller (BET) theory. Mean particle size (D_{BET}) was calculated from the BET data according to the equation proposed by Ikegami and co-workers [14], which assumes that the particles are closed sphere with smooth surface and uniform size.

Differential thermal analysis and thermogravimetry (TG/DTA; Rigaku Thermalplus TG 8120, Tokyo, Japan) were used to study the exo–endo temperature of the dried $Ce_{0.8}Nd_{0.2}O_{1.9}$ precursor. A heating rate of 10 °C/min was used in both the DTA and TG measurements up to 600 °C in air. Infrared spectra of $Ce_{1-x}Nd_xO_{2-(1/2)x}$ (x = 0.05–0.25) powders prepared by coprecipitation and calcined at 600 °C were recorded in the 400–4000 cm^{-1} range by preparing KBr (Merck for spectroscopy) pellets (5 wt% sample).

The morphological features of the NDC sintered pellets were observed using a scanning electron microscope (SEM; Hitachi S-3500H, Tokyo, Japan). All specimens were polished with a series of emery paper of 800, 1000, 1200, and 1500 grit. Contamination on the surface was ultrasonically cleaned with ethanol. Finally thermal etching was carried on all specimens at 1400 °C for 30 min. In order to define clearly the grain size, we use the lineal intercept technique to determine the grain size [15]. The average grain size, G_a, was calculated using the following relation: $G_a = 1.5L/MN$, where 1.5 is a geometry-dependent proportionality constant [16], L is the total test line length, M is the magnification, and N is the total number of intercepts.

The total electrical conductivity is the sum of the contributions of oxygen ions, electrons and holes. However, under the experimental conditions in this study, the contributions of electrons and holes are negligible. The ionic conductivity of NDC was measured by a two-point DC method on dense sintered pellet specimens, 12 mm diameter and 2 mm thick. The ionic conductivity measurements were made at various temperatures in the range of 500–800 °C in 1 atm air. Silver served as the electrodes, and was pasted on both sides of the pellet. Arrhenius plots (plots of $\log\sigma$ vs. $10^3/T$) were constructed and activation energies for conduction were computed. Activation energy for conduction is obtained by plotting the ionic conductivity data as an Arrhenius relation for thermally activated conduction, and was calculated according to following equation:

$$\sigma T = \sigma_o \exp\left(-\frac{E_a}{kT}\right) \tag{2}$$

where E_a is the activation energy for conduction, T is absolute temperature, and σ_o is a pre-exponential factor [17].

The densities of the sintered samples were measured by the Archimends method. The theoretical densities, ρ_{th} (kg/m^3) of NDC were calculated using

$$\rho_{th} = \left(\frac{4}{N_A a^3}\right)[M_{Ce}(1-x) + M_{Nd}(x) + M_O(2-0.5x)] \tag{3}$$

where M_{Ce}, M_{Nd}, and M_O are the molecular weights of the subspecies in kg/mol, N_A is Avogadro's number (6.023×10^{23}/mol), and a is the XRD lattice parameter. Neodymium was assumed to be in the 3+ valence states [18].

The thermal expansion coefficients of sintered $Ce_{0.8}Nd_{0.2}O_{1.90}$ pellets were measured by dilatometer (DIL; Model Netzsch DIL 402 PC, Bavaria, Germany) using a constant heating rate of 10 °C/min in the temperature range of 35–800 °C.

Vickers hardness was measured using a microhardness tester (Akashi MVK-H110, Tokyo, Japan) with the load of 9.8 N, held for 10 s. At least 10 indentations were used to obtain the mean and standard deviation value of hardness and fracture toughness. The Vickers indentation hardness was determined by using the average length of both diagonals and calculated using the follow relationship: $H_V = 1.8544(P/d^2)$ where P is the load (N), and d is the mean value of both diagonals (μm). The fracture toughness versus crack size was determined using the equation of Anstis et al. [19]:

$$K_{IC} = 0.016\left(\frac{E}{H_V}\right)^{1/2}\left(\frac{P}{C^{3/2}}\right) \quad (4)$$

where K_{IC} is fracture toughness, E is Young's modulus (205 GPa for Gd-doped ceria solid solution [20]), H_V is Vickers hardness, P is the load, and C is the half crack size. The crack length of $2C$ is measured from the two ends of the cracks propagated from the corners of an indentation. There are many indentation equations for the calculation of K_{IC} as reviewed by (see Fig. 8) Poton and Rawling [21], with specific conditions and limitation for using these formulae. So far no universal formula is available to evaluate K_{IC} for all ceramics materials [22]; for convenience, in this study the equation of Anstis et al. [19] was used to determine K_{IC} of our NDC samples.

3. Results and discussion

Fig. 1 shows the DTA/TG trace of the as-dried precursor for $Ce_{0.8}Nd_{0.2}O_{1.9}$. The first weight loss between 50 and 100 °C is associated with an endothermic peak at ~80 °C in the DTA curve. It is ascribed to the loss of molecular water absorbed on the $Ce_{0.8}Nd_{0.2}O_{1.9}$ precursor. The second abrupt weight loss, between 250 and 400 °C, is correlated with a small exothermic peak at ~270 °C and an endothermic peak at ~295 °C, caused mainly by the oxidation and the decomposition of cerium-based hydrate, respectively. Finally, the weight of the as-dried precursor appears nearly constant above 450 °C, which indicates that beyond this temperature a single phase of $Ce_{0.8}Nd_{0.2}O_{1.9}$ is present without any impurities such as hydrate and nitrate material at this stage.

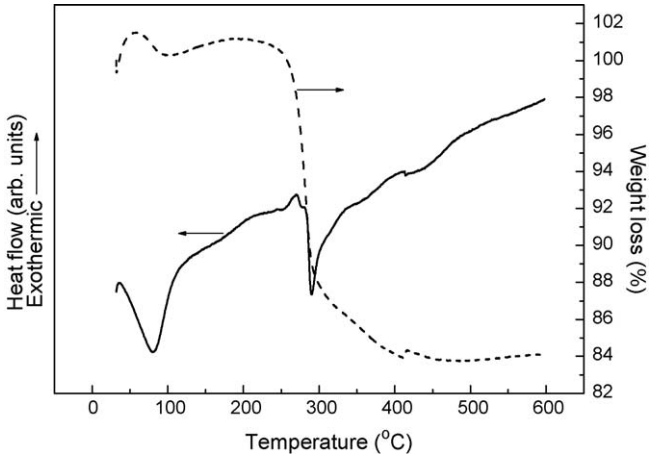

Fig. 1. The TG/DTA curves for a $Ce_{0.8}Nd_{0.2}O_{1.9}$ precursor.

IR spectra of the neodymium-doped ceria powders prepared by coprecipitation and calcined at 600 °C are compared in Fig. 2. The major features in the IR spectra are bands in the 1250–1750 and 3250–3750 cm^{-1} regions. The band due to the stretching frequency of Ce–O can be seen in the 840–860 cm^{-1} region. The bands in the frequency region from 1250 to 1750 cm^{-1} are assigned to carbonate species formed by coordination of CO_2 molecules onto the coordinately neodymium-doped ceria powder's surfaces [23]. The band in the 3000–3800 cm^{-1} region can be attributed to O–H-stretching of physiosorbed H_2O or from Ce–OH surface groups. There are no significant differences in these five powders. This lack of difference indicates that $Ce_{1-x}Nd_xO_{2-(1/2)x}$ solid solutions have been formed, a result which is in complete accord with the X-ray diffraction analysis.

The X-ray diffraction patterns of the NDC ceramics sintered at 1500 °C are shown in Fig. 3, and shows that the NDC ceramics contain only the cubic fluorite structure with space group $Fm3m$ (JCPDS powder diffraction file No. 34-0394). No secondary phases were observed in any specimens, indicating a complete solid solution for the NDC dopant concentration range and sintering condition studied here. The introduction of Nd_2O_3 into CeO_2 can cause a small shift in the X-ray peak reflections to lower 2θ values which is indicative of an increase in lattice parameter. Fig. 4 shows the cubic lattice parameter of $Ce_{1-x}Nd_xO_{2-(1/2)x}$ ceramics as a function of dopant concentration, for $x = 0.05$–0.25. The lattice parameter increased with increasing neodymium content, as a result of the different Ce^{4+}

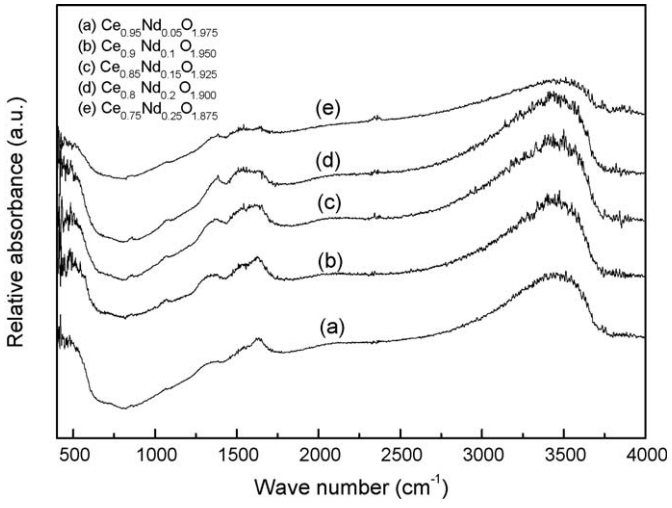

Fig. 2. Infrared spectra of NDC powders prepared by coprecipitation and calcined at 600 °C for 2 h.

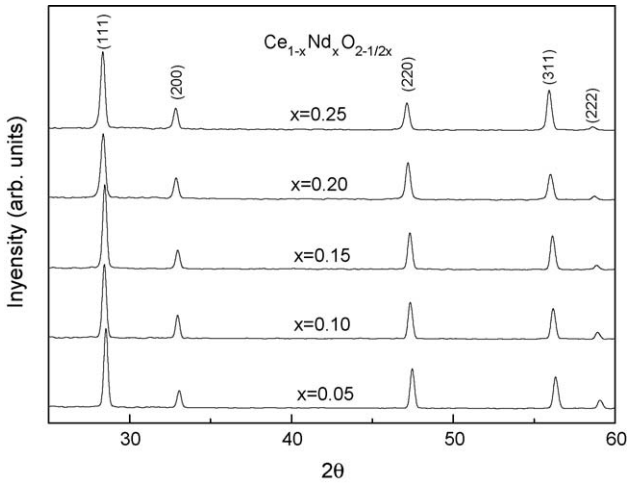

Fig. 3. XRD patterns of NDC ceramics sintered at 1500 °C for 5 h.

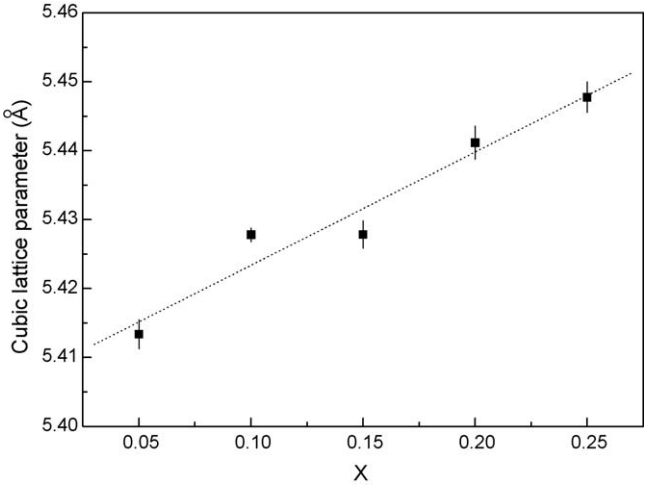

Fig. 4. Cubic lattice parameter of NDC powders as a function of x.

(0.096 nm) and Nd^{3+} (0.111 nm) radii in solid solutions of a fluorite-type structure. Doping Nd in CeO_2 lattice will induce elastic strain in the lattice as the Nd content is increased. This effect causes the lattice plane spacing to change and the diffraction peaks to shift to new 2θ position. As shown in Fig. 4, as the Nd content increases, the cubic lattice parameter increases linearly as $a(x) = 5.4069 + 0.1642x$ for $Ce_{1-x}Nd_xO_{2-(1/2)x}$ (x = 0.05–0.25) powders, indicating that these solid solutions obey Vegard's rule.

The mean particle size (D_{BET}) and crystallite size (D_{XRD}) of NDC powders calcined at 600 °C are listed in Table 1. It is well known, $\phi = D_{BET}/D_{XRD}$ is a factor which reflects the agglomeration extent of the primary crystallites [14]. For neodymium-doped ceria powders, D_{XRD} and D_{BET} values show unexpected discrepancies at various Nd dopant contents. D_{BET} values are always larger than D_{XRD} value, which is assumed due to a small amount of agglomeration occurring in NDC powders, resulting in a situation where N_2 gas cannot completely penetrate agglomerates during BET analysis. Moreover, XRD can detect the grain size comprising the agglomerates within particles. The ϕ value is distributed from 1.00 to 1.38 in NDC powder.

Table 1
Surface area, particle size (D_{BET}), and crystallite size (D_{XRD}) for NDC powders calcined at 600 °C for 2 h.

Composition	Surface area (m^2/g)	D_{BET} [a] (nm)	D_{XRD} [b] (nm)	ϕ [c]
x = 0.05	39.45	20.8	17.5	1.18
x = 0.10	38.60	21.2	17.7	1.19
x = 0.15	40.27	20.1	20.1	1.00
x = 0.20	31.25	25.8	18.7	1.38
x = 0.25	33.23	24.1	20.7	1.16

[a] Particle size (D_{BET}) measured from specific surface area.
[b] Crystallite size (D_{XRD}) measured from XRD line broadening.
[c] ϕ = particle size (D_{BET})/crystallite size (D_{XRD}).

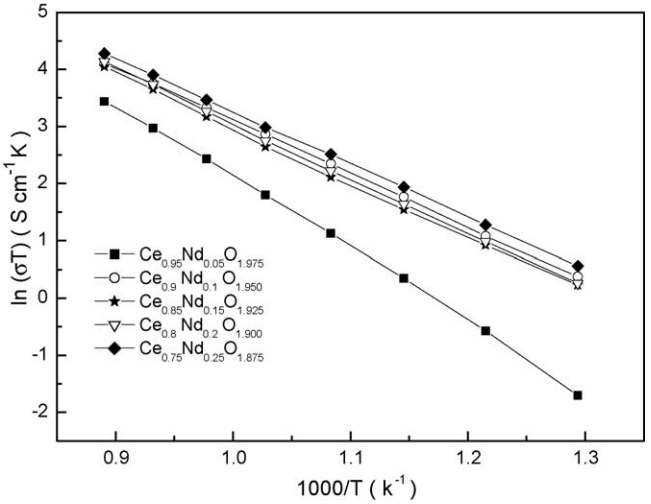

Fig. 5. Arrhenius plots for ionic conductivity of NDC ceramics.

$Ce_{0.8}Nd_{0.2}O_{1.9}$ powder showed the highest ϕ value among NDC powders; this may be due to the highest amount of agglomeration occurring in the $Ce_{0.8}Nd_{0.2}O_{1.9}$ powder.

The Arrhenius plot for the ionic conductivity of NDC is shown in Fig. 5. The ionic conductivity is the bulk value, which is the sum of the grain interior, and grain boundary contributions [24]. Pure ceria is a poor ion conductor ($\sigma_{800°C} \sim (0.24 \pm 0.02) \times 10^{-3}$ S/cm). The ionic conductivity is significantly enhanced in neodymium-doped ceria ceramic by increasing oxygen vacancies ($V^{\bullet\bullet}_O$). The ionic conductivity of neodymium-doped ceria increases systematically with increasing neodymium substitution and reaches a maximum for the composition of $Ce_{0.75}Nd_{0.25}O_{1.875}$ ($\sigma_{800°C} \sim 4.615 \times 10^{-2}$ S/cm). As temperature increases, the oxide ion mobility increases, and consequently the conductivity increases at high temperatures. Activation energy for conduction is obtained by plotting the ionic conductivity data in the Arrhenius relation for thermally activated conduction. The activation energies are distributed in the range of 0.794–1.093 eV. The minimum activation energy, E_a = 0.794 eV, was found in the $Ce_{0.75}Nd_{0.25}O_{1.875}$ specimen. This result is ascribed to the fact that the change of short-range and/or long-range ordering defect is associated with the increase of the dopant concentration [25]. With increasing doping level, defect association between the effectively positively charged oxygen vacancies ($V^{\bullet\bullet}_O$) and the negatively charged dopant

Table 2
Ionic conductivity and activation energy for NDC ceramics.

Composition	Conductivity ($\times 10^{-2}$ S/cm), 800 °C	Activation energy, E_a (eV)
$x = 0.05$	1.823	1.093
$x = 0.10$	3.964	0.802
$x = 0.15$	3.590	0.820
$x = 0.20$	3.909	0.829
$x = 0.25$	4.615	0.794

cations (N'_{ce}) can change from dimmers to trimmers (*i.e.* the amount of defect association is regulated by positively charged oxygen vacancies and negatively charged dopant cations) and then defect clusters [25]. In addition, some microdomains of some possible ordered intermediate phase could also form. These different defects structures will affect the defect energetics and the activation energy. A summary of ionic conductivities, and activation energies of NDC ceramics are listed in Table 2.

Apart from high ion conductivity, the electrolyte materials for SOFC must have close matched thermal expansion coefficients for cathode and anode materials to avoid microcracking between the electrodes and electrolyte at the operating temperatures. Consequently, thermal expansion is an important property, which governs the performance of high-temperature devices. Fig. 6 shows the plot of linear thermal expansion (in percent) as function of temperature, and indicates a linear thermal expansion fitted as a function of temperature using a polynomial regression. The polynomial correlations are given as follows (temperature, T, in centigrade):

For $Ce_{0.8}Nd_{0.2}O_{1.9}$:

$$100(\Delta L/L_o) = -0.03297 + (6.65364 \times 10^{-4})T + (1.94722 \times 10^{-6})T^2 - (1.56301 \times 10^{-9})T^3 + (5.56307 \times 10^{-13})T^4$$

The thermal expansion coefficient for the $Ce_{0.8}Nd_{0.2}O_{1.90}$ specimen was found to be 15.57 ppm/°C. Similar phenomenon

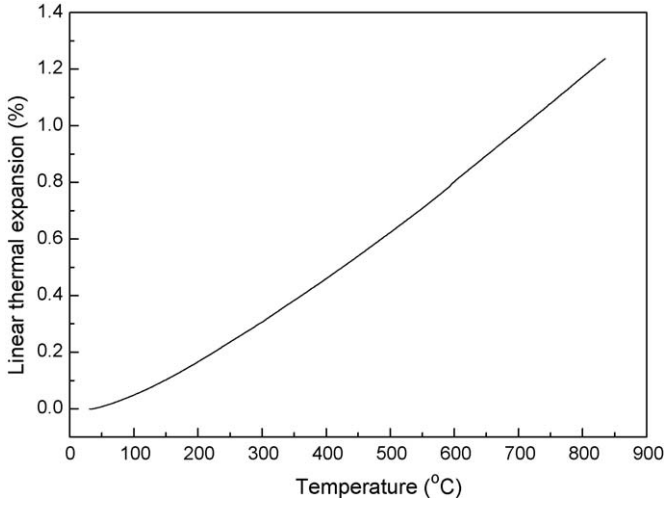

Fig. 6. Linear thermal expansion of $Ce_{0.8}Nd_{0.2}O_{1.9}$ ceramic as a function of temperature in the temperature range of 30–800 °C.

are observed in the $Ce_{1-x}Nd_xO_{2-(1/2)x}$ ($x = 0.05, 0.10, 0.15$, and 0.25) specimens. The thermal expansion coefficient of NDC is close to that of $La_{0.8}Sr_{0.2}Co_{0.2}Fe_{0.8}O_3$ cathode material (15.40 ppm/°C) [26]. The anode materials used, usually metal nickel, is mixed with the electrolyte materials. Therefore, anode thermal expansion coefficients are also close to the electrolyte. We conclude that as the thermal expansion coefficients of all three fuel cell components are very close, it is anticipated that microcracking should not occur as a result of SOFC operation.

Microstructures of NDC ceramics sintered at 1500 °C are shown in Fig. 7, and indicate good densification with grain sizes in the range of 3–7 μm. In the dopant range $0.05 \leq x \leq 0.20$, the grain size is in the range of 3.45–4.12 μm (Table 3). However, for the sample where $x = 0.25$, the grain size was observed to increase significantly to 7.54 μm. This observation may indicate that for $x \geq 0.25$ NDC can exhibit significantly enhancing grain growth. The NDC sintered samples were all greater than 95% theoretical density. There are some papers reported on the grain size of gadolinia-doped ceria with various synthesis techniques and sintering conditions. For example, Cheng et al. [27] proposed that the grain size of $Ce_{0.9}Gd_{0.1}O_{1.95}$ ceramics prepared by the gel-casting process sintered at 1500 °C for 5 h was about 5 μm. Zhang et al. [10] proposed that the grain sizes of $Ce_{0.8}Gd_{0.2}O_{2-\delta}$ ceramics prepared via a homogenous precipitation method using hexamethylenetetramine as a precipitant sintered at 1400 °C for 3 h were in the range of 0.5–9.5 μm. Gil et al. [28] proposed that the grain sizes of $Ce_{0.9}Gd_{0.1}O_{2-\delta}$ ceramics prepared via a solid-state reaction technique, which incorporated with 0.2–2.0 wt.% Bi_2O_3 sintered at 1600 °C without holding time were in the range of 2.8–3.4 μm. Perez-Coll et al. [29] proposed that the grain sizes of $Ce_{1-x}Gd_xO_{2-\delta}$ ($x = 0.05$–0.30) ceramics prepared via a freeze-drying precursor method sintered at 1600 °C for 10 h were in the range of 4.4–7.0 μm. Chourashiya et al. [30] proposed that the grain sizes of $Ce_{1-x}Gd_xO_{2-\delta}$ ($x = 0.10$–0.30) ceramics prepared via a solid-state reaction technique sintered at 1500 °C for 2 h were in the range of 2.0–3.0 μm. It is concluded that grain size of gadolinia-doped ceria is dependent on the process, sintering temperature, and soaking time. In the dopant range $0.05 \leq x \leq 0.20$ for $Ce_{1-x}Nd_xO_{2-(1/2)x}$, the grain sizes are in the range of 3.45–4.12 μm, which are correspondences between the literature reports and this study.

Fig. 8 shows a typical microstructure and indentation crack pattern used to determine microhardness (H_V) and fracture toughness (K_{IC}). In this study, if there are no cracks happening in specimens, we assume that $d = 2C$ is used to determine fracture toughness (K_{IC}).

Table 3 shows the indentation fracture toughness and microhardness data for NDC ceramics sintered at 1500 °C. The results indicate that for the range of NDC compositions studied here, all possessed similar microhardness, in the range of 5.454–7.978 GPa. The microhardness, as measured, appeared to be independent of neodymium-dopant content and grain size. The hardness of a solid is generally defined as its resistance to local deformation [31]. According to previously reported results, pure CeO_2 exhibits a fracture toughness of ~1.5 MPa $m^{1/2}$ [32]. Trivalent, NDC ceramics exhibited a

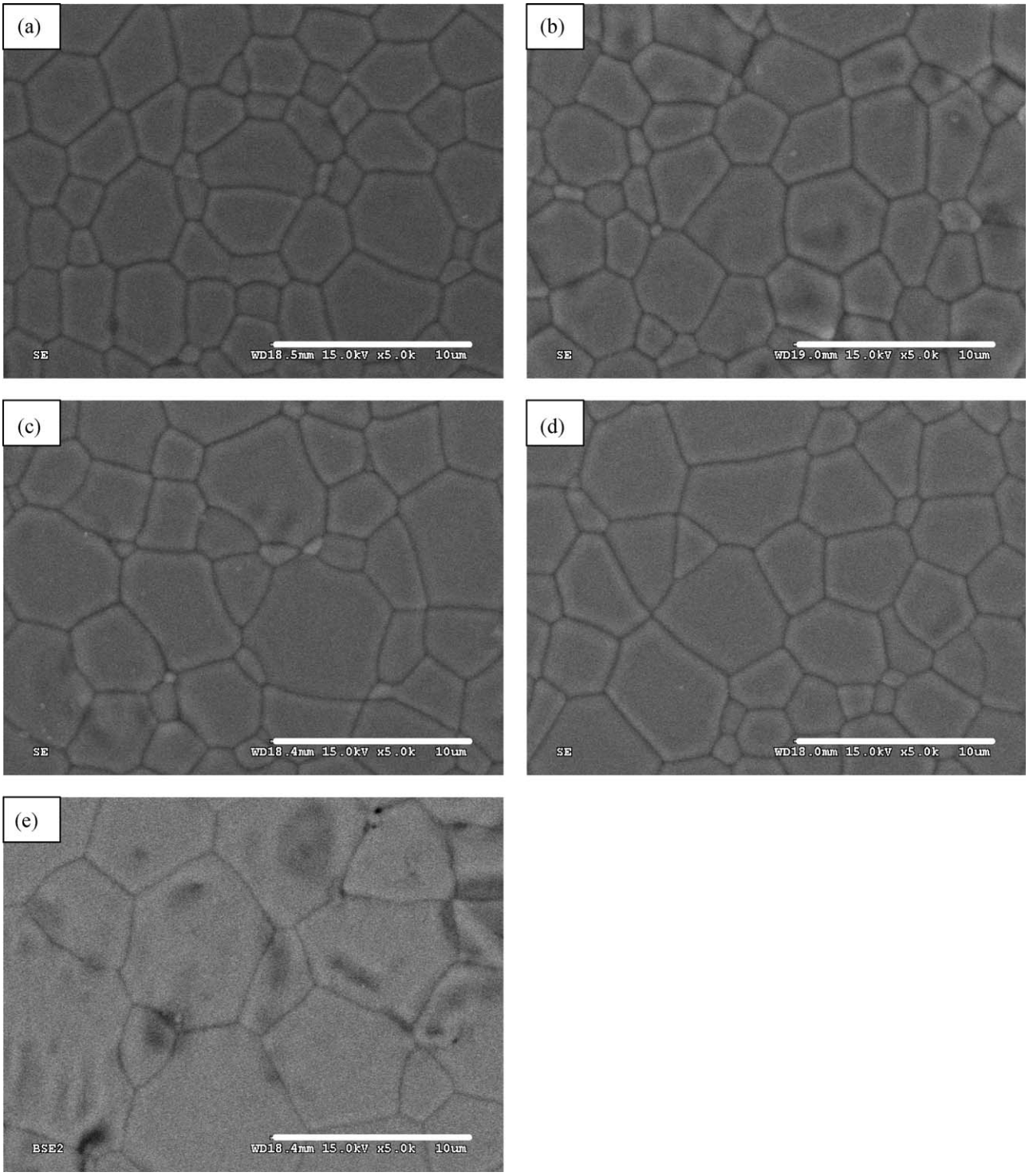

Fig. 7. Typical grain sizes of NDC ceramics sintered at 1500 °C for 5 h: (a) $x = 0.05$, (b) $x = 0.10$, (c) $x = 0.15$, (d) $x = 0.20$, and (e) $x = 0.25$.

fracture toughness ~4–5 times higher than pure ceria, with a distribution range of 6.236–6.846 MPa $m^{1/2}$. These results indicate that the addition of neodymium into CeO_2 has significantly improved the fracture properties. Such high indentation fracture toughness of NDC may be due to a number of toughening mechanisms based on crack deflection by grain boundaries [33], generate porosity and reduction in Young's modulus. This is due to the fact that porosity is a phase which should be considered when making sensible mechanical properties such as microhardness and fracture toughness. As the porosity reduced, the microhardness and fracture toughness increased. The detailed indentation fracture toughness and microhardness data are summarized in Table 3. In this study, the microhardness and fracture toughness increase showed the same tendency, which both scales with the density, *i.e.* a reduction in porosity.

Table 3
Density, grain size, indentation fracture toughness and microhardness for NDC ceramics as function of Nd content.

Composition	Theoretical density (g/cm^3)[a]	Density (%)	Grain size (μm)	Microhardness, H_V (GPa)	Fracture toughness, K_{IC} (MPa m$^{1/2}$)[b]
$x = 0.05$	7.198	95.11	3.55	5.454 ± 0.091	6.236 ± 0.021
$x = 0.10$	7.133	96.49	3.56	7.978 ± 0.107	6.846 ± 0.017
$x = 0.15$	7.125	95.87	4.12	7.285 ± 0.087	6.704 ± 0.027
$x = 0.20$	7.065	95.38	3.45	6.799 ± 0.105	6.590 ± 0.046
$x = 0.25$	7.031	95.64	7.54	7.058 ± 0.126	6.650 ± 0.030

[a] Calculated based on Eq. (3).
[b] Calculated based on Eq. (4).

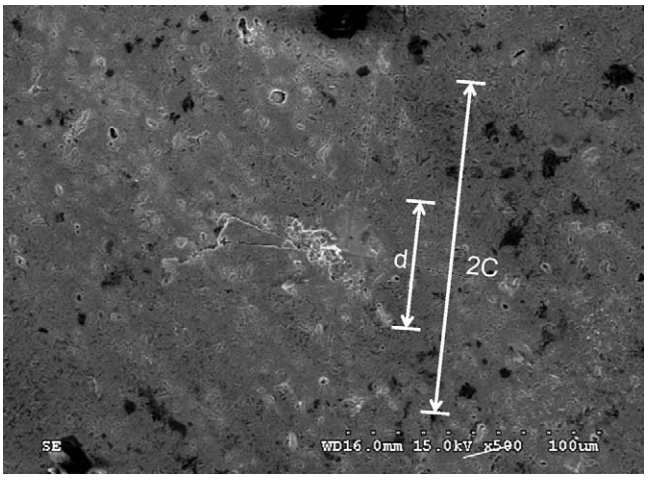

Fig. 8. Typical microstructure, porosity distribution and indentation crack patterns used to determined microhardness (H_V) and fracture toughness (K_{IC}).

4. Summary and conclusions

In this study, we have synthesized neodymium-doped ceria ($Ce_{1-x}Nd_xO_{2-(1/2)x}$; x in the range 0.05–0.25) powders of nano dimensions and high specific surface areas are in the range of 31.25–40.27 m^2/g. The powder particle size ranged from 20.1 to 25.8 nm, in which the crystallite size varied from 17.5 to 20.7 nm. For NDC powders sintered at 1500 °C for 5 h, the maximum ionic conductivity, $\sigma_{800°C} = 4.615 \times 10^{-2}$ S/cm with minimum activation energy, $E_a = 0.794$ eV, occurred at $Ce_{0.75}Nd_{0.25}O_{1.875}$ ceramic. The grain size of NDC ceramic remained constant at $x = 0.2$ and tended to increase with neodymium-dopant content at $x = 0.25$. Neodymium as dopant added to ceria was observed to significantly enhance grain growth, increasing the grain size from about 3.55 to 7.54 μm when x was increased about 0.20–0.25. NDC ceramics revealed high fracture toughness, the fracture toughness distribution was in the range of 6.236–6.846 MPa m$^{1/2}$. The high fracture toughness of NDC was attributed to crack deflection. Moreover, the porosity may significantly influence the microhardness and fracture toughness. As the porosity is reduced, the microhardness and fracture toughness are increased. The ion conductivity of $Ce_{0.75}Nd_{0.25}O_{1.875}$ is higher than the most commonly used solid electrolyte, yttrium-stabilized zirconia at 800 °C. We conclude that the $Ce_{0.75}Nd_{0.25}O_{1.875}$ composition is suitable for solid oxide fuel cells applications.

Acknowledgement

The authors would like to thank the National Science Council of Taiwan for financially supporting this research under Contract No. NSC 96-2221-E-259-005.

References

[1] X.T. Su, Q.Z. Yan, X.H. Ma, W.F. Zhang, C.C. Ge, Effect of co-dopant addition on the properties of yttrium and neodymium doped barium cerate electrolyte, Solid State Ionics 177 (2006) 1041–1045.
[2] N.Q. Minh, Ceramic fuel cells, J. Am. Ceram. Soc. 76 (1993) 563–588.
[3] H.L. Tuller, A.S. Nowick, Defect structure and electrical properties of nonstoichiometric CeO_2 single crystals, J. Electrochem. Soc. 126 (1979) 209–217.
[4] W. Hung, P. Shuk, M. Greenblatt, Properties of sol–gel prepared $Ce_{1-x}Sm_xO_{2-x/2}$ solid electrolytes, Solid State Ionics 100 (1997) 23–27.
[5] E.K. Chang, R.N. Blumenthal, The nonstoichiometric defect structure and transport properties of CeO_{2-x} in the near-stoichiometric composition range, J. Solid State Chem. 72 (1988) 330–337.
[6] H. Inaba, H. Tagawa, Ceria-based solid electrolytes, Solid State Ionics 83 (1996) 1–16.
[7] H. Yahiro, K. Eguchi, H. Arai, Electrical properties and reducibilities of ceria–rare earth oxide system and their application to solid oxide fuel cell, Solid State Ionics 36 (1989) 71–75.
[8] K. Eguchi, T. Setoguchi, T. Inoue, H. Arai, Electrical properties of ceria-based oxides and their application to solid oxide fuel cells, Solid State Ionics 52 (1992) 165–172.
[9] T. Zhang, Z. Zeng, H. Huang, P. Hing, J. Kliner, Effect of alumina addition on the electrical and mechanical properties of $Ce_{0.8}Gd_{0.2}O_{2-\delta}$ ceramics, Mater. Lett. 57 (2002) 124–129.
[10] T.S. Zhang, J. Ma, L.B. Kong, P. Hing, J.A. Kilner, Preparation and mechanical properties of dense $Ce_{0.8}Gd_{0.2}O_{2-\delta}$ ceramics, Solid State Ionics 167 (2004) 191–196.
[11] H. Li, C. Xia, M. Zhu, Z. Zhou, G. Meng, Reactive $Ce_{0.8}Sm_{0.2}O_{1.9}$ powder synthesized by carbonate coprecipitation: sintering and electrical characteristics, Acta Mater. 54 (2006) 721–727.
[12] T.S. Zhang, J. Ma, L.H. Luo, S.H. Chan, Preparation and properties of dense $Ce_{0.9}Gd_{0.1}O_{2-\delta}$ ceramics for use as electrolytes in IT-SOFCs, J. Alloys Compd. 422 (2006) 46–52.
[13] H.P. Klug, L.E. Alexander, X-ray Diffraction Procedures, Wiley, New York, 1974.
[14] J.G. Li, T. Ikegami, Y. Wang, T. Mori, 10-mol%-Gd_2O_3-doped CeO_2 solid solution via carbonate coprecipitation: a comparative study, J. Am. Ceram. Soc. 86 (2003) 915–921.
[15] J.C. Wurst, J.A. Nelson, Lineal intercept technique for measuring grain size in two-phase polycrystalline ceramics, J. Am. Ceram. Soc. 55 (1972) 109.
[16] M.I. Mendelson, Average grain size in polycrystalline ceramics, J. Am. Ceram. Soc. 52 (1969) 436–443.

[17] C. Tian, S.W. Chan, Ionic conductivities, sintering temperatures and microstructures of bulk ceramic CeO_2 doped with Y_2O_3, Solid State Ionics 134 (2000) 89–102.
[18] X.D. Zhou, W. Huebner, H.U. Andersion, Processing of nanometer-scale CeO_2 particles, Chem. Mater. 15 (2003) 178–182.
[19] G.R. Anstis, P. Chantikul, B.R. Lawn, D.B. Marshall, A critical evaluation of indentation techniques for measuring fracture toughness. I. Direct crack measurements, J. Am. Ceram. Soc. 64 (1981) 533–538.
[20] A. Argoitia, J.F. Baumard, C. Gault, in: P. Vincenzini (Ed.), High Tech. Ceram., Elsevier, 1987, p. 1381.
[21] B.C. Poton, R.D. Rawling, Vickers indentation fracture toughness test. Part 1. Review of literature and formulation of standard indentation toughness equations, Mater. Sci. Technol. 5 (1989) 865–872.
[22] J. Ma, T.S. Zhang, L.B. Kong, P. Hing, Y.J. Leng, S.H. Chan, Preparation and characterization of dense $Ce_{0.8}Y_{0.15}O_{2-\delta}$ ceramics, J. Eur. Ceram. Soc. 24 (2004) 2641–2648.
[23] V. Bolis, G. Magnacca, G. Cerrato, C. Morterra, Microcalorimetric and IR-spectroscopic study of the room temperature adsorption of CO_2 on pure and sulphated t-ZrO_2, Thermochim. Acta 379 (2001) 147–161.
[24] S. Zha, C. Xia, G. Meng, Effect of Gd(Sm) doping on properties of ceria electrolyte for solid oxide fuel cells, J. Power Sources 115 (2003) 44–48.
[25] W. Chen, A. Navrotsky, Thermochemical study of trivalent-doped ceria systems: CeO_2–$MO_{1.5}$ (M = La, Gd, and Y), J. Mater. Res. 21 (2006) 3242–3251.
[26] L.W. Tai, M.M. Nasrallah, H.U. Anderson, D.M. Sparlin, S.R. Sehlin, Structure and electrical properties of $La_{1-x}Sr_xCo_{1-y}Fe_yO_3$. Part 2. The system $La_{1-x}Sr_xCo_{0.2}Fe_{0.8}O_3$, Solid State Ionics 76 (1995) 273–283.
[27] J.G. Cheng, S.W. Zha, J. Huang, X.Q. Liu, G.Y. Meng, Sintering behavior and electrical conductivity of $Ce_{0.9}Gd_{0.1}O_{1.95}$ powder prepared by the gel-casting process, Mater. Chem. Phys. 78 (2003) 195–791.
[28] V. Gil, J. Tartaj, C. Moure, P. Duran, Sintering, microstructural development, and electrical properties of gadolinia-doped ceria electrolyte with bismuth oxide as a sintering aid, J. Eur. Ceram. Soc. 26 (2006) 3161–3171.
[29] D. Perez-Coll, P. Nunez, J.C. Ruiz-Moralse, J. Pena-Martinez, J.R. Frade, Re-examination of bulk and grain boundary conductivities of $Ce_{1-x}Gd_xO_{2-\delta}$ ceramics, Electrochim. Acta 52 (2007) 2001–2008.
[30] M.G. Chourashiya, J.Y. Patil, S.H. Pawar, L.D. Jadhav, Studies on structure, morphological and electrical properties of $Ce_{1-x}Gd_xO_{2-(x/2)}$, Mater. Chem. Phys. 109 (2008) 39–44.
[31] Y.J. He, A.J.A. Winnubst, C.D. Sagel-Ransijn, A.J. Burggraaf, H. Verweij, Enhanced mechanical properties by grain boundary strengthening in ultra-fine-grained TZP ceramics, J. Eur. Ceram. Soc. 16 (1996) 601–612.
[32] S. Mashina, O. Shaizero, S. Meriani, Mechanical properties in the ceria–zirconia system, J. Eur. Ceram. Soc. 9 (1992) 127–132.
[33] M.W. Barsoum, Fundamentals of Ceramics, The McGraw-Hill Companies, Singapore, 1997, p. 418.